FastFlood Hydraulics: Exponentially cascaded cross-sectional volume estimates from elevation data.

B. van den Bout[1], V. Glas[1]

[1]Twente University, Faculty of Geo-information Science and Earth Observation

Corresponding author: B. van den Bout, b.vandenbout@utwente.nl

Abstract

Fastflood is a methodology and platform for rapid flood assessment which is freely available on the fastflood.org website. The web-based simulation tool employs several key techniques to speed up flood simulation up to 1500 times compared to conventional flood models. In this article, we continue the verification and development of the method by validating hydraulic behavior in fluvial setting. In the final step of the Fastflood method, peak discharge estimates are used to reconstruct a peak flood depth field. The original method is improved with an efficient algorithm for cross-sectional estimates of discharge-volume relationships. Two study cased are presented, the Koshi River in North Nepal, and the Rhine river at the border between Germany and the Netherlands. For these areas the discharge-volume relationship is compared for a full 2D hydrodynamic model, the Fastflood method and an estimate through Mannings equation using cross-sectional area and wetted perimeter. We observe a similar match between the model setups, with deviations within a 5% percent range. There is an excellent estimation of general flow depths with the improved FastFlood methodology. Moreover, the application of a localized estimate of Manning's flow law can provide flow velocities, but limitations remain due to the absence of inertia in the Fastflood model.

Introduction

Rapid tools for flood simulation provide utility in rapid assessment, forecasting, and sketching of mitigation design. Recently a variety of approaches have been developed to find useful balances between efficiency and accuracy. In example, empirical approaches such as susceptibility mapping through random forest approaches (Abedi et al., 2022). Other methods mimic the physics of water flow more closely, such as the cellular automata developed by Jamali et al. (2019) or Guidolin et al. (2016). The machine learning research field shows a heavy focus on generalized neural networks for generating flood maps and forecasts (Mosavi et al., 2018; Oliviera et al., 2023). However, until now, spatial dependencies in the flood process create difficulties and site or event-specific training remains a requirement. Physically-based methods approach the efficiency problem by leveraging assumptions about the physical system. Optimizing the meshing of the model domain, using 1d-2D coupling or quad-tree approaches, can benefit computation speed (Bout & jetten, 2018; Kalyanapu et al., 2011; Dahm et al., 2014). The Fastflood method is a similar physically-based approach that uses steady-state flow estimates to avoid computing full dynamics of an event.

The original Fastflood method as presented in (Bout et al., 2023) was calibration and validated on various study-cases based on flood extent, and later on discharge values. These approaches showed some shortcomings related to the diverse aspects and usages of flood models. In some cases, flood extent might be the primary variable of interest. However, for flood mitigation design some accuracy guarantees are required for flow depths and velocities in fluvial setting. Flood extent is predominantly guided by the terrain and flood depths, therefor it gives some indication of correct flood depth estimates (Neal et al., 2015). Despite this, a more thorough analysis of the flow depths and velocities is required. Comparative analysis with existing methodologies for various discharge values and fluvial settings contribute to the further validation the FastFlood methodology.

For this comparative analyses, two types of existing and frequently used hydraulic models are used; 2D/3D hydrodynamic modelling and cross-sectional hydraulic models. The hydrodynamic models solve the partial differential equations governing water flow in 2D (Saint-Venant Equations) or 3D (Navier-Stokes Equations). These sets of equations include mass and momentum continuity laws, as well as all relevant sources and transfers of momentum between the fluids and surrounding objects (Delestre et al., 2017). This results in highly detailed output, but heavy computational cost. The performance of hydrodynamic models is predominantly limited by the accuracy of the input data (de Arruda Gomes et al., 2021).

Cross-sectional models relate discharges and flow heights in a more computational efficient manner by utilizing Mannings Law which relates discharge to the cross-sectional area and wetted perimeter (Te Chow et al., 1988). In particular for engineering purposes, this approach has a long history of excellent application (Bjerklie et al., 2005). However, its performance depends on the availability of sufficient cross-sectional data (Praminik et al., 2010). Cross-sectional models (E.g. Hec-RAS, SOBEK), do have limitations relating to cross-sectional spacing, non-linear effects and non-homogeneity in river morphology, but generally show excellent fit with observations and full models (Brunner, 2016; Dhondia & Stelling, 2004).

Objective

In this work, we compare the Fastflood methodology, and its renewed algorithm to produce flood depths from peak discharges, with existing standards such as 2D hydrodynamic modelling and Mannings Law. We analyze its behavior in predicting peak flow depths as well as peak flow velocities in two fluvial settings; The Rhine river on the border between Germany and the Netherlands, and the Koshi river in Nepal.

Methodology

FastFlood

The Fastflood model and methodology was introduced by Bout et al. (2023). In this paragraph a short overview of the model setup is given. The model contains 5 key steps, with critical underlying assumptions. The steps are as follows;

1. **Terrain correction**

   Using a Fast Sweeping Algorithm, gridcells in the elevation model are forced to be at least the elevation of the lowest neighbor, with some additional small value. The resulting elevation model is monotonically increasing.

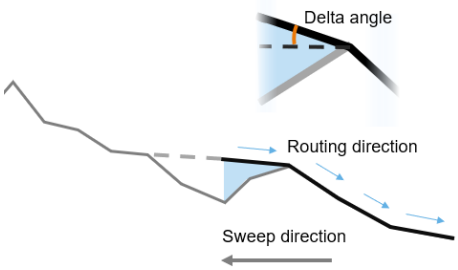

Figure 1 Terrain hydro-correction

2. **Flow network derivation**

   The monotonically increasing elevation model can be used to create a flow network by taking the local derivatives of the elevation and using the angle of steepest descent as a flow direction. Optionally, these angles might be limited to 4 or 8 directions to mimic a D4 or D8 flow direction network.

3. **Steady-state discharge routing**

   Over this network, a steady-state discharge is routed through a simple flow accumulation, with another speed up by using fast sweeping numerical algorithms.

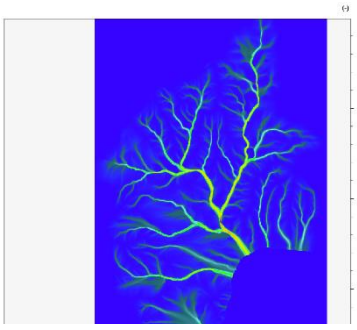

Figure 2 Steady-state discharge routing

4. **Partial steady-state correction**

   Natural events rarely reach a steady-state flow. Based on catchment properties and event duration, a correction is applied to estimate Actual peak flow.

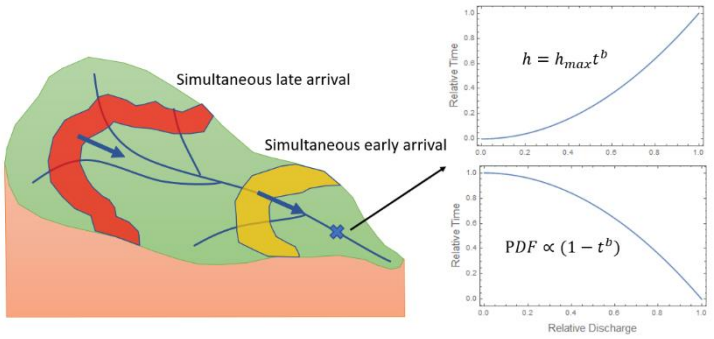

Figure 3 Partial steady state correction based on flow distance distributions

5. **Flow depth reconstruction**

   Finally, peak flow rates are used to reconstruct a spatial peak flow depth field (flood map). This step used an inversion of Mannings equations for a rectangular channel. In this research, a revision on this inversion is introduced with significant improvements.

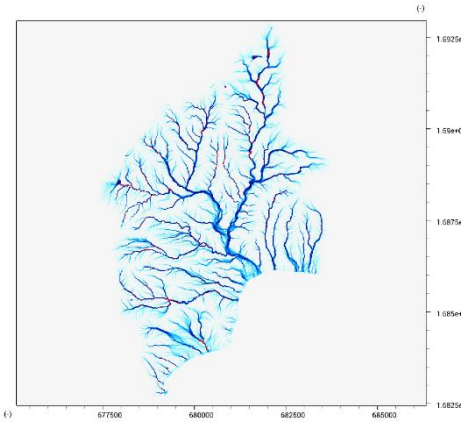

Figure 4 Flow depth reconstruction

The key assumptions which are taken in the methodology relate to the non-dynamic nature of the algorithms. Only peak discharges, flow depths and velocities are estimated. As a result, input of precipitation is required in a duration-intensity pair, and cannot be a full rainfall graph. The steady-state assumption used in step 3 is corrected in step 4, but the correction step relies on various assumptions about catchment homogeneity. For more details on the derivation of this correction see Bout et al., (2023).

Flow depth reconstruction

The original flow depth reconstruction, which is analyzed in this work, consists of two steps. First, the local flow volumes are estimated based on the discharge. For a rectangular channel, an analytical solution of Mannings equation is used to estimate the local flow height based on the width and discharge through a channel. Mannings equation for a rectangular channel was inverted. Such an approach was described in the original work on the FastFlood method (Equation 1).

$$\mathrm{h} = \left(\frac{\mathrm{q}}{w}\frac{n}{\sqrt{s}}\right)^{\frac{3}{5}} \qquad 1$$

Where h is an approximation of channel flow height (m), q is the discharge (m3/s), w is the channel width (m), n is the Mannings surface roughness coefficient for the river bed ($\frac{s}{m^{\frac{1}{3}}}$), and s is the slope gradient (m/m).

The downside to this approach is that the rectangular channel had to be either parameterized manually, or a fixed value must be chosen that did generally not represent the variation in channel topography.

In this article, we will replace this step by using an exponentially cascaded cross-sectional volume estimate that will be introduced below.

In the second step of the flow depth reconstruction, the water volume is spatially re-distributed according to the topography and physically-based consistency. A diffusive-wave flow solver is used to move the water from the channel pixels throughout the model domain. In this diffusive-wave solver only gravitational, pressure and frictional flow are considered (Equation 2 & 3).

$$h_{i+1} = h_i + dt\left(\frac{d(h_i u_x)}{dx} + \frac{d(h_i u_y)}{dy} + max(0, R - I)\right) \quad 2$$

$$u_x = \sqrt{\frac{h^{\frac{3}{2}}}{n}\left(-\frac{dz}{dx} - \frac{d\left(\frac{1}{2}h^2\right)}{dx}\right)} \qquad u_y = \sqrt{\frac{h^{\frac{3}{2}}}{n}\left(-\frac{dz}{dx} - \frac{d\left(\frac{1}{2}h^2\right)}{dx}\right)} \quad 3$$

Where $u_x \; and \; u_y$ are the (artificial) velocities in the x and y directions (m/s), R is the precipitation rate (m/s), I is the infiltration rate (m/s), dx is the grid cell spacing (m), z is the terrain elevation (m).

For this final step, a new alternative solution strategy is proposed in the following section.

Exponentially-cascaded cross-sectional volume estimates from elevation data

In this paragraph explains the improved method which substitutes the analytical solution of Mannings equation in the flow depth reconstruction. The estimation of local flow height, volume or cross-sectional area results in a two-way dependency. Mannings formula is widely used in hydraulic engineering, and expresses this relationship as equation 4.

$$Q = A * V = A * \left(\frac{1}{n}\right)\left(\frac{A^{\frac{2}{3}}}{P} S^{\frac{1}{2}}\right) \quad 4$$

Where Q is the discharge in m^3/s, A is the cross-sectional area in m^2, n is the Manning Coefficient (s/m1/3), P is the wetted perimeter of the cross-sectional flow and S is the hydraulic gradient (m/m).

When the flow rate (discharge) increases, water heights and velocities both increase as well. The resulting equation must be solved to find an appropriate wetted perimeter and cross-sectional area in order to accurately estimate the local flow volume. Both of these depend on the flow height and the geometry of the channel, and both influence the velocities as well.

We efficiently solve this problem by introducing the following algorithm. For a given discharge path, we start by considering the trapezoid channel that exists between the gridcell where the discharge is routed, together with two neighbors. For this small trapezoid segment, a solution is found for the wetted perimeter and cross-sectional area. If these are contained within the height of trapezoid, these values are used directly. If not, we iterate, where for each iteration, a new trapezoid is constructed around the existing one, using more neighbors.

We exponentially grow the steps, such that for an iteration I, the 3^i x3î grid is searched, centered a distance of 3^i gridcells removed from the gridcell under consideration. The direction of these grid samples is determined by the slopes calculated of the corners of an orthorectangular placed grid of size 3^I.

The algorithm is partially visualized in figure 5. Here, the samples are all taken to the left and right, while in actuality, the algorithm uses the slope directions to place the sample grids for each iteration.

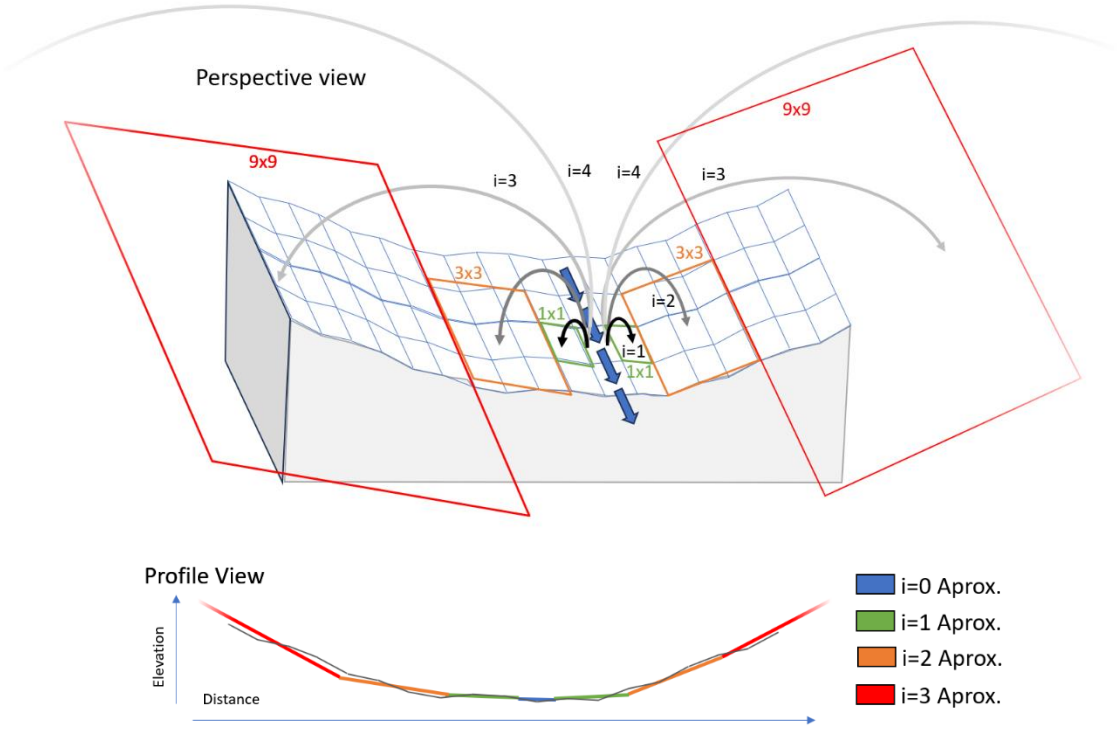

Figure 5 A schematic indication of the exponentially cascading profile approximation, in perspective view (top) and profile view (bottom).

Because of the exponentially cascading nature of the approximation, the number of calculations steps can be limited, allowing for efficient execution. Within our numerical implementation, we further re-use the average elevation values calculated during the previous steps. This means that for each step, only a 9-value average must be calculated for each pixel.

Study Case

We verify and analyze the behavior and dynamics of the Fastflood model on two study-sites. Both are Riverine systems which are subject to extreme discharge events.

Rhine River

The Rhine river is the largest river to flow into the Netherlands, and is fed predominantly by groundwater and snowmelt from Germany, Switzerland and France. The area of focus is several kilometers of river stretch near Lobith, on the border between the Netherlands and Germany. At this location an average discharge of about 2300 m^3/s is measured, before splitting into the upper and lower Rhine branches (Euhlinger et al., 2009). High-resolution bathymetric data was obtained from the Dutch ministry of

infrastructure and water, with a resolution of 1x1 meter, covering most of the river bed. The channel width is about 450 meters on average, with depths over 6 meters. We resampled this data to 10 meter resolution using spatial averaging to benefit calculation time and match a more typical application. In figure 6 and 7 the cross sectional area of the case-study region is presented.

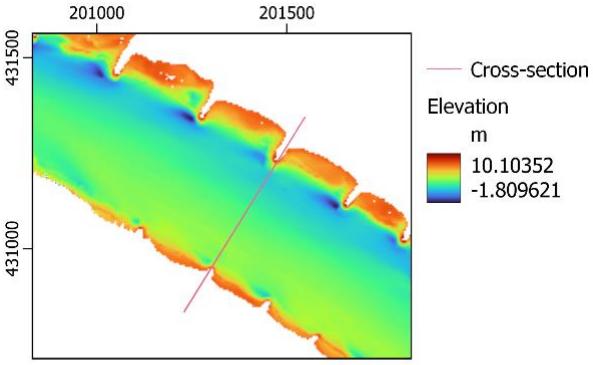

Figure 6 The bathymetric data for a piece of the Rhine river.

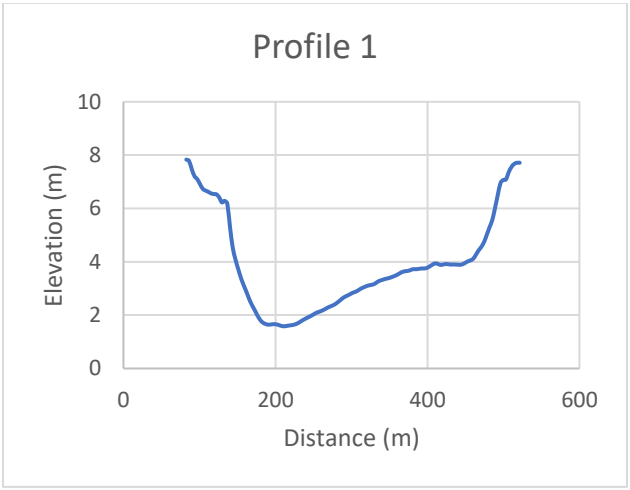

Figure 7 The cross-sectional profile in the Rhine river, location indicated in figure 6.

The SunKoshi river, a tributary of the Koshi river, feeds into Nepal from the Tibetan highlands and the central and northern Nepalese Mountains. A combination of snowmelt and monsoonal rainfall cause regular flooding issues in this area. Due to the steep landscape, roads, villages and the river channel are all located in close proximity to the valley bottom. According to monthly discharge data records, an average discharge of approximately 200 m^3/s enters this area. Elevation data was obtained from commercial WorldDEM Neo 5 meter resolution DTM products. For this site, two cross-sections are chosen, one with a steeper slope (0.081 m/m) and one with a more gentle slope (0.0241 m/m), to reflect the variety of river steepness in the area.

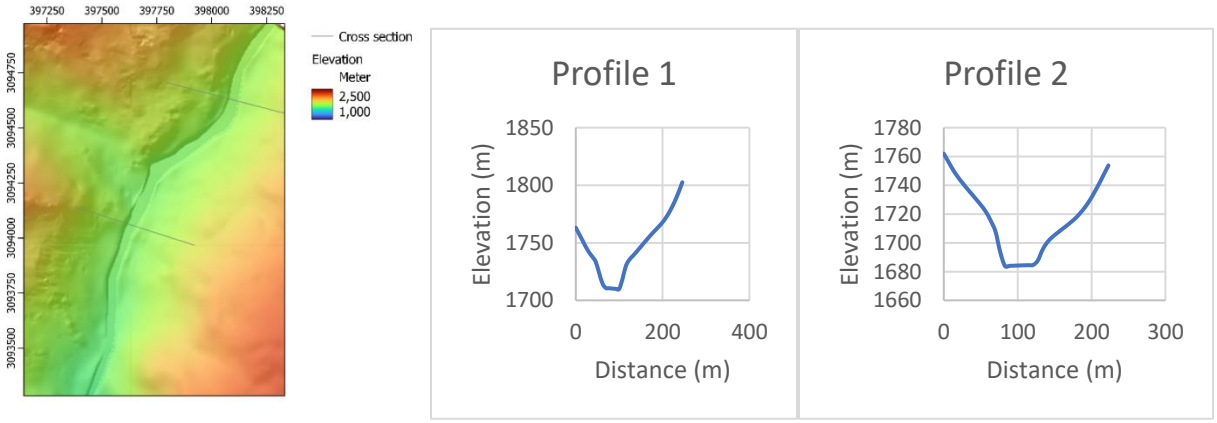

Figure 8 The elevation data for the SunKoshi river, sourced from WorldDEM Neo 5m. Two profiles are indicated and shown (middle and right).

Setup

We simulate discharge extremes using three methods;

i) Mannings Equation, using wetted perimeter and cross-sectional area to derive stage-discharge relationships
ii) Saint-Venant equations as implemented in the open-source LISEM simulation software.
iii) The FastFlood method revised method, using cascaded profile approximation as available on the www.fastflood.org simulation platform.

Several discharge input boundary conditions are simulated. Because of the limited extent of the bathymetric data, we only use values that stay within the profile data for the Rhine study site. Comparison of the models will be based on inter-model comparison; Stage-discharge relationships will be compared using R-squared.

The Mannings N was considered homogeneous over the river profiles, with a value of n=0.04 chosen for the Rhine study site and 0.05 chosen for Koshi river based on the USGS field manual for selecting Mannings Surface Roughness. For the Koshi study site, the Mannings values outside of the river bed were determined by using the WorldCover 10m dataset from Copernicus, where each land use class is then linked with a reference value from the USGS field manual. This allows for a more detailed analysis of stage-discharge relationships between the models.

In the LISEM setup, the discharge boundary condition was linked at each timestep (dt = 0.1 second, sub-timestep iterations are active) and distributed over the cross-section of the inner river bed. The upstream boundary was set as a closed boundary condition, where-as the downstream boundary condition was left open. The discharge boundary condition is left constant for a steady flow to develop.

In the Fastflood setup, we use monodirectional channel routing, 250 iterations for the flow depth reconstructions and a maximum of 5 iterations for the cascading profile approximations. The results will show performance and comparison with the 2D hydrodynamic simulation in uncalibrated and calibrated state. For calibration, we minimize the RMSE between the flow depths resulting from the hydrodynamic and Fastflood model using a brute-force approach on Mannings N. We show both calibrated and uncalibrated comparison to represent relative and absolute differences and magnify the differences in behavior.

Results and discussion

Figure 9 shows the stage-discharge relationships derived from the three model setups. While showing a good match, some notable differences are present. Please note we are not calibrating here based on actual observations. By altering parameter values for Mannings coefficient a more optimal fit with data might be obtained. Currently, results are shown to highlight the behavior of various modelling techniques.

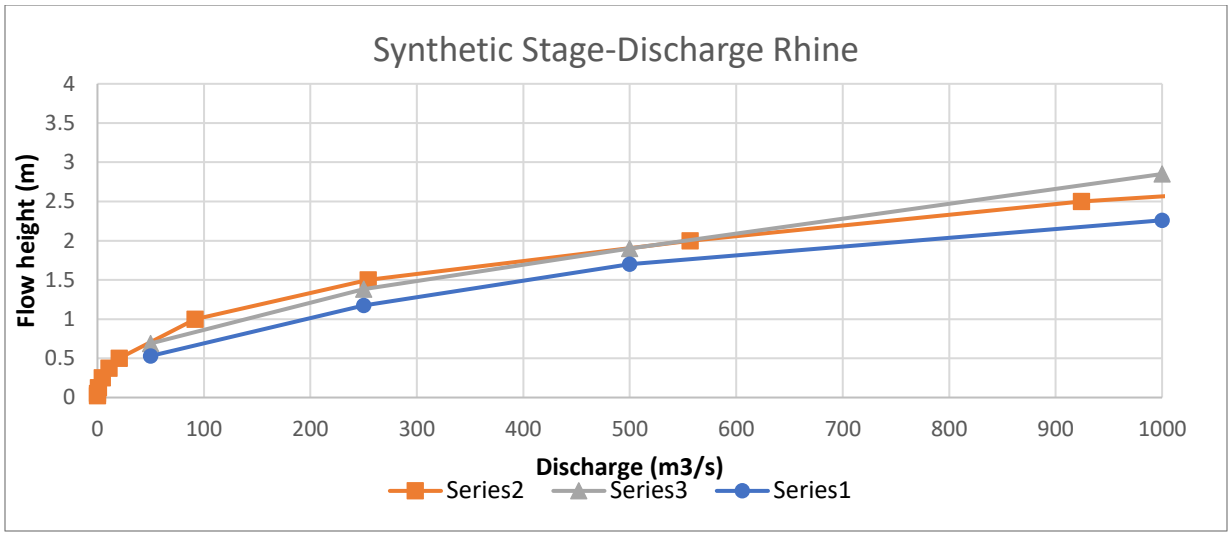

Figure 9 Stage discharge relationship for the three models for the Rhine study-case.

The Fastflood results show good fit with full simulation (R2=0.983, Pearson coefficient = 0.992), as well as with Mannings equation.

Figure 10 shows the flow depth results and difference from the hydrodynamic simulation as well as the Fastflood method. The first example shows an uncalibrated comparison, where-as the second example shows the output from the models when the Fastflood method is calibrated on the results of the hydrodynamic simulation.

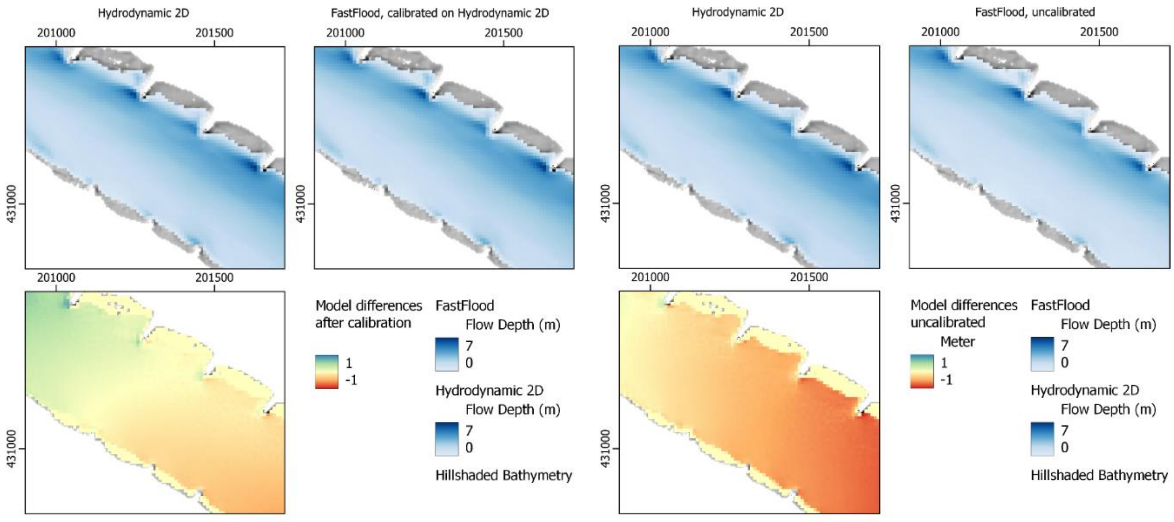

Figure 10 Left) Comparison of full hydrodynamic 2D flood depth solution and a calibrated FastFlood simulation (calibrated on the 2d hydrodynamic solution). Right) Comparison of full hydrodynamic 2D solution and a uncalibrated FastFlood simulation.

The results show a good replication of flow depths throughout the area, with deviations on average below 12%. The differences of the calibrated model show that a significant part of the differences is caused by how the models handle the boundary conditions. The open boundary condition in the 2D hydrodynamic model does not instantiate an initial flow velocity, which results in additional accumulation of water at the

start (South-East) of the river section. Finally, the FastFlood method contains a closed boundary condition during its final step of water redistribution. During this step, water is also slightly moved downstream, resulting in some accumulation to the North-West side of our river section. The simulation of a longer river section might minimize these problems. Additionally, a boundary area might be introduced with a length of around 20 pixels to avoid these effects in analysis of model results.

Figure 11 shows the peak velocities resulting from the hydrodynamics and FastFlood simulations respectively.

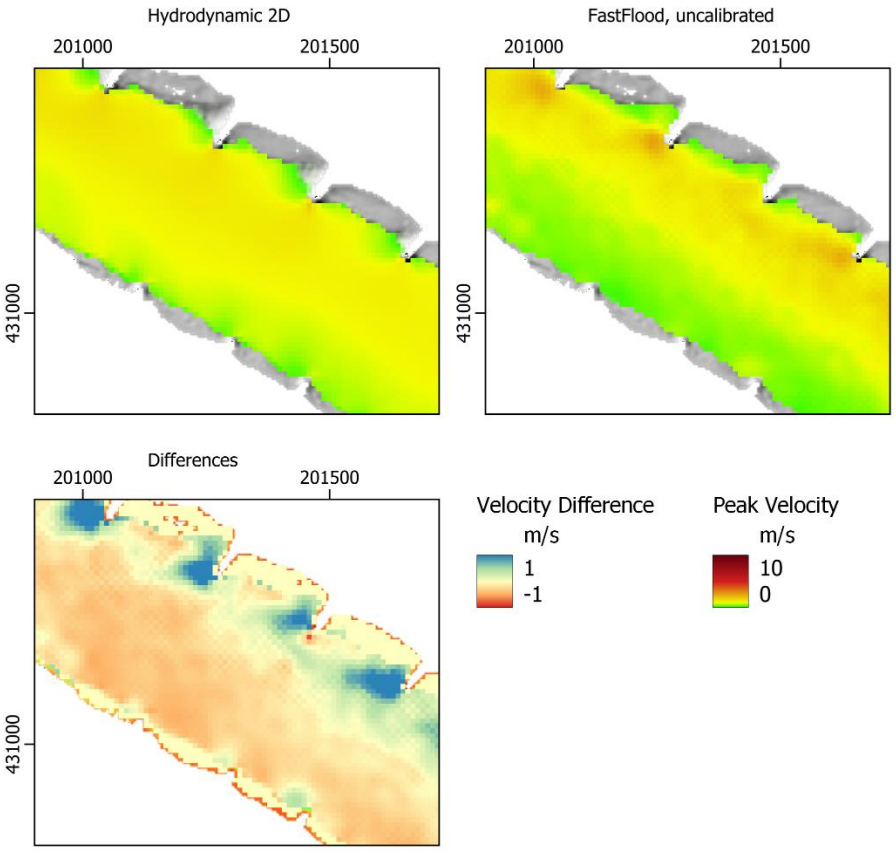

Figure 11 Peak velocities from the hydrodynamic 2d modelling solution and the fastflood model, and their absolute differences.

Similar to the flow height patterns, we see a good fit between the spatial flow velocity patterns predicted by the Fastflood method and the 2D hydrodynamic simulation. Both models generally predict similar velocities, with larger flow velocities in the North side of the river. Fastflood over-estimates these differences. In addition, the regularly spaced groynes in the channel result in lower velocities in the 2D hydrodynamic model, as water is forced to flow through the middle section of the river. In the Fastflood model, higher velocities are predicted directly based on hydraulic gradient and depth. Thus, the lack of inertial forces in changing topography results in deviations in estimated model velocities. These results indicate that usage of these model results in morphological studies is not possible, as important effects of reverse currents and inertial dynamics are lacking in the Fastflood model results. Similarly, mitigation

measures that depend on flow velocities must not use a spatial estimation, but instead rely on the profile-based estimated produced by the method.

Figure 12 shows the stage-discharge relationships derived from the three model setups for the 2 Koshi river cross-sections.

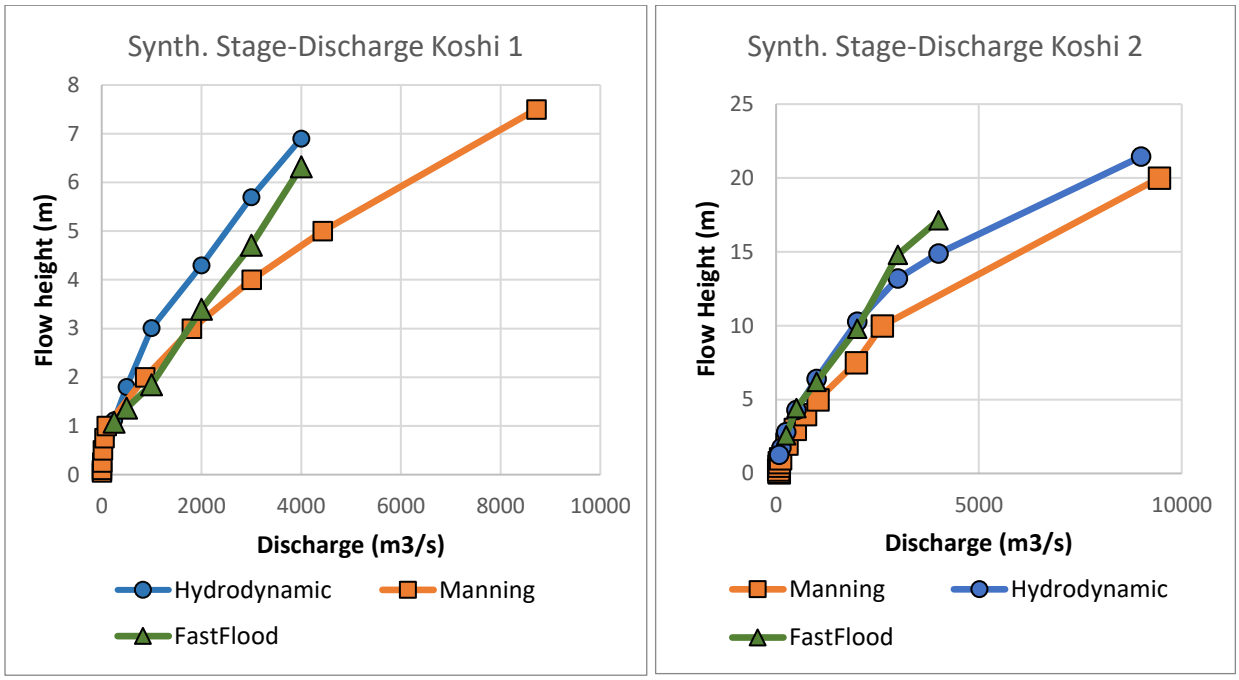

Figure 92 Stage-discharge relationships using various modelling methods for the two profiles in the Sunkoshi River.

Again, the Fastflood results show good correlations with the full simulation as well as with Mannings equation. For the first profile, a slightly worse fit is found (R2=0.970, Pearson coefficient = 0.984) when compared with the second profile location (R2 = 0.986, Pearson coefficient = 0.993).

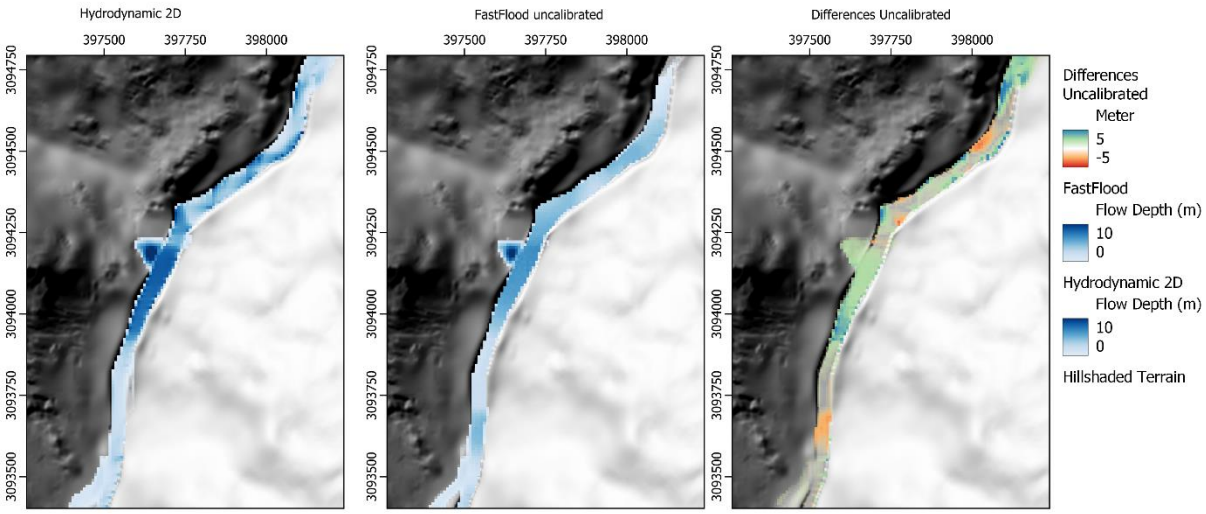

Figure 13 Flow depth results and differences, comparing hydrodynamic 2d modelling and the FastFlood method in the steep Sunkoshi river.

When considering the spatial variation, the influence of the steep, and varying slopes in the landscape and river bed have significant effects on the flow depth variations. The central area, with more gentle slope, immediately has higher flow depths in both the 2D hydrodynamic and Fastflood simulations. Near cross-section 1 (North) and the South area, steeper slopes results in shallower flow heights. These variations explain the lower accuracy fit found for cross-section 1 in the stage-discharge relationships.

An additional difference can be observed in the steep Northern section. Here, the 2D hydrodynamic simulation predicts that the rapidly moving water has lateral patterns within the extent of the valley bottom as it gains momentum and reflects of the channel sides. This is visible within the northern section of the flow heights shown in figure 15. In reality, at these scales such behavior might be significantly reduced due to energy dissipation in increased turbulence. The causes of this are however not reflected in these kinds of lower-resolution elevation data. Such effects, originating from the inertial effects of waters movement, are not present in the Fastflood results, where the lateral variation in flow depths is typically minimal if the river bed topography is homogeneous. Half-way the river section, the depression in the valley side is filled accurately by the Fastflood method.

Figure 14 shows the flow velocities for the Koshi river, using either Full hydrodynamic 2d modelling or the FastFlood method with an inverse Manning equation using water-surface level slopes.

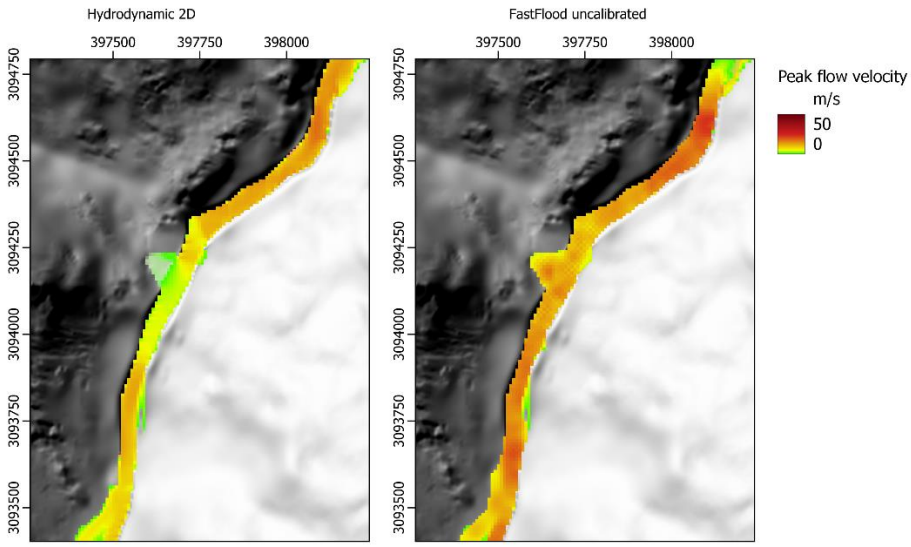

Figure 14 A comparison of flow velocities in the Sunkoshi river as predicted by both full hydrodynamic 2D flow modelling and the fastflood method.

Fastflood reflects some of the velocity variations accurately, such as the increased velocity due to steeper slopes, as well as the reductions in wider sections of the river. For the depression in the valley side, half-way our study-site, a major difference can be noticed. Where the 2D hydrodynamic simulation predicts a local entrapment of the water, with significantly reduced velocity, the Fastflood methodology simply follows local hydraulic slope and flow depths, and over-predicts flow velocities.

Conclusions

Our results show a good fit in flood depth and flow velocities between the Fastflood model and full hydrodynamic simulation. Additionally, R2 values indicate a good fit with the Mannings equation as well.

Concerning spatial flow heights, the different models present hydraulically consistent results. However, both models deal differently with the influences of inflow and outflow boundaries. This causes the increase and decrease of flow heights up to 10%.

The exponentially-cascaded cross-sectional approximation aids flow height accuracy by estimating local water volumes from peak discharges. Nevertheless, several limitations remain, such as the lack of inertial behavior in steep rivers. Consequently, , there are significant differences in predicted peak flow velocities, and minor differences in flow height patterns, in particular for the Koshi case-study,.

Additionally, the developed flow depth reconstruction step in the FastFlood model works well if the pixel width of the channel does not exceed the number of chosen iterations. This allows the water to spread and the algorithm to converge. Such considerations mean that caution about the underlying assumptions of the model is warranted. In order to increase the efficiency of this step further, additional research might study using the cascaded profile approximation to distribute the water spatially. Finally, improvements in speed might still be gained from a multi-resolution modelling approach and GPU acceleration.

Finally, a more detailed assessment of the influence of the presented algorithm on embankments must be carried out. When these are located at some distance from the stream center, the profile at the embankments might be approximated by averaging the terrain over a larger area. This effectively lowers the heights of the embankments in the approximate cross-sectional profiles, which can be expected to influence behavior. Alternative approaches to the exponentially-cascaded cross-sectional approximation might be attempted. These approaches involve some tracking measure of maximum heights to estimate the transferability of water over the floodplains due to obstacles and embankments.

References

Abedi, R., Costache, R., Shafizadeh-Moghadam, H., & Pham, Q. B. (2022). Flash-flood susceptibility mapping based on XGBoost, random forest and boosted regression trees. *Geocarto International*, *37*(19), 5479-5496.

Bjerklie, D. M., Dingman, S. L., & Bolster, C. H. (2005). Comparison of constitutive flow resistance equations based on the Manning and Chezy equations applied to natural rivers. *Water resources research*, *41*(11)

Bout, V. B., & Jetten, V. G. (2018). The validity of flow approximations when simulating catchment-integrated flash floods. *Journal of hydrology*, *556*, 674-688.

Brunner, G. W. (2016). HEC-RAS River Analysis System: Hydraulic Reference Manual, Version 5.0. *US Army Corps of Engineers–Hydrologic Engineering Center*, *547*.

Dahm, R., Hsu, C. T., Lien, H. C., Chang, C. H., & Prinsen, G. (2014, November). Next generation flood modelling using 3Di: A case study in Taiwan. In *DSD international conference*.

Delestre, O., Darboux, F., James, F., Lucas, C., Laguerre, C., & Cordier, S. (2017). FullSWOF: Full Shallow-Water equations for overland flow. *Journal of Open Source Software*, *2*(20), 448.

DHONDIA, J. F., & STELLING, G. S. (2004). Sobek one dimensional–two dimensional integrated hydraulic model for flood simulation–its capabilities and features explained. In *Hydroinformatics: (In 2 Volumes, with CD-ROM)* (pp. 1867-1874).

de Arruda Gomes, M. M., de Melo Verçosa, L. F., & Cirilo, J. A. (2021). Hydrologic models coupled with 2D hydrodynamic model for high-resolution urban flood simulation. *Natural Hazards*, *108*(3), 3121-3157.

Uehlinger, U. F., Wantzen, K. M., Leuven, R. S., & Arndt, H. (2009). The Rhine river basin. Rivers of Europe, Academic Proceedings, London.

Guidolin, M., Chen, A. S., Ghimire, B., Keedwell, E. C., Djordjević, S., & Savić, D. A. (2016). A weighted cellular automata 2D inundation model for rapid flood analysis. *Environmental Modelling & Software*, *84*, 378-394.

Jamali, B., Bach, P. M., Cunningham, L., & Deletic, A. (2019). A Cellular Automata fast flood evaluation (CA-fffé) model. *Water Resources Research*, *55*(6), 4936-4953.

Kalyanapu, A. J., Shankar, S., Pardyjak, E. R., Judi, D. R., & Burian, S. J. (2011). Assessment of GPU computational enhancement to a 2D flood model. *Environmental Modelling & Software*, *26*(8), 1009-1016.

Neal, J. C., Odoni, N. A., Trigg, M. A., Freer, J. E., Garcia-Pintado, J., Mason, D. C., ... & Bates, P. D. (2015). Efficient incorporation of channel cross-section geometry uncertainty into regional and global scale flood inundation models. *Journal of Hydrology*, *529*, 169-183.

Mosavi, A., Ozturk, P., & Chau, K. W. (2018). Flood prediction using machine learning models: Literature review. *Water*, *10*(11), 1536.

Oliveira Santos, V., Costa Rocha, P. A., Scott, J., Thé, J. V. G., & Gharabaghi, B. (2023). A New Graph-Based Deep Learning Model to Predict Flooding with Validation on a Case Study on the Humber River. *Water*, *15*(10), 1827.

Pramanik, N., Panda, R. K., & Sen, D. (2010). One dimensional hydrodynamic modeling of river flow using DEM extracted river cross-sections. *Water Resources Management*, *24*, 835-852.

Te Chow, V., Maidment, D. R., & Mays, L. W. (1988). *Applied hydrology*.

Van den Bout, B., Jetten, V. G., van Westen, C. J., & Lombardo, L. (2023). A breakthrough in fast flood simulation. *Environmental Modelling & Software*, *168*, 105787.